Revista Mexicana de Astronomía y Astrofísica, **42**, 23–39 (2006)

LOW REDSHIFT BAL QSOS IN THE EIGENVECTOR 1 CONTEXT

J. W. Sulentic,[1] D. Dultzin-Hacyan,[2] P. Marziani,[3] C. Bongardo,[3] V. Braito,[3] M. Calvani,[3] and R. Zamanov[3,4]

Received 2005 February 22; accepted 2005 November 7

RESUMEN

Intentamos caracterizar la geometría de los cuasares con líneas anchas de absorción (cuasares BAL por sus siglas en inglés) estudiando una muestra de bajo corrimiento al rojo, e identificamos 12 de ellos. Encontramos que la mayoría de estas fuentes son cuasares de población A (FWHM de H$\beta \leq 4000$ km s^{-1}, Sulentic et al. 2000a). Una posible correlación entre la velocidad terminal y la magnitud absoluta en V sugiere que la razón de la luminosidad bolométrica a la masa del hoyo negro es un factor determinante, con los valores máximos para los BAL clásicos. La emisión de C IV en los BAL clásicos muestra un perfil con corrimiento al azul, lo que apoya el escenario de un viento que fluye hacia afuera de un disco con un ángulo de apertura media menor de 50 grados. La observación de características secundarias de "mini-BAL" en los perfiles de emisión de C IV nos ha motivado a modelar los cuasares BAL con una componente relacionada al gas que produce las líneas anchas de emisión y que produce un flujo hacia afuera del disco de acreción y coaxial con éste.

ABSTRACT

We attempt to characterize the geometry of Broad Absorption Line (BAL) QSOs by studying a low redshift sample of 12 sources. We find that the majority of these sources are Population A quasars as defined in Sulentic et al. (2000a, broad Hβ FWHM$\leq$ 4000 km s^{-1}). A possible correlation between terminal velocity and absolute V magnitude suggests that the bolometric luminosity to black hole mass ratio $L_{\rm bol}/M_{\rm BH}$ is a governing factor with classical BAL sources showing the highest values. CIVλ1549 emission in classical BAL sources shows a profile blueshift that supports a disk wind/outflow scenario with a half opening angle of $\lesssim 50^{\circ}$. Observation of "secondary" mini-BAL features in the CIVλ1549 emission profile motivates us to model BALs with an additional component that may be involved with the BLR outflow and co-axial with the accretion disk.

Key Words: **GALAXIES: ACTIVE — QUASARS: ABSORPTION LINES — QUASARS: EMISSION LINES**

1. INTRODUCTION

Type 1 Active Galactic Nuclei (AGNs) apparently show three kinds of associated absorption features (here we focus on CIVλ1549 as a characteristic high ionization line, HIL).

1. Narrow absorption lines (NALs) are the most common and are accepted as "associated" (e.g., Vestergaard 2003) (1) if they lie within $\pm$5000 km s^{-1} of the CIVλ1549 emission line centroid, (2) if the rest frame equivalent width is between 0.5 and $\approx$ 4.0 Å, (3) if the line width is no more than a few 100 km s^{-1}(or alternatively the CIVλ1549 doublet is resolved in absorption), and/or (4) if the lines are variable in intensity (Richards et al. 1999; Brandt, Laor, & Wills 2000; Ganguly et al. 2001; Verstergaard 2003; Wise et al. 2004).

2. Broad absorption lines (BALs) are thought to occur in 15% – 20% of AGNs (Hewett & Foltz

[1]Department of Physics and Astronomy, University of Alabama, USA.
[2]Instituto de Astronomía, Universidad Nacional Autónoma de México, México, D. F., México.
[3]INAF, Osservatorio Astronomico di Padova, Italy.
[4]National Astronomical Observatory, Bulgaria.

2003; Reichard et al. 2003) and generally show blueshifted troughs with velocity widths of several thousands km s^{-1} and equivalent widths of several tens of Å. Terminal velocities in these broad features are measured in tens of thousands km s^{-1}.

3. Absorption features with intermediate properties (FWHM few thousand km s^{-1}, EW $\sim 5-10$ Å and sometimes variable) are called "mini-BALs" and may be even rarer than BALs (Jannuzi et al. 1998; Narayan et al. 2004).

It is tempting to relate mini-BALs to BALs because they show blueshift velocities up to $\sim$ 50,000 km s^{-1}, overlapping the BAL range, although there are arguments against a close connection (e.g., Narayan et al. 2004). However, mini-BALs are regarded as intrinsic (i.e., due to gas physically close to, and dynamically affected by, the active nucleus central engine) absorption features, and not just as "associated" like NALs, which could be also due to distant gas). In this paper we consider BAL and mini-BAL phenomenology in low redshift quasars, while only occasional consideration will be given to NALs.

The discovery of BAL and mini-BAL QSOs has always been biased toward AGNs with high enough redshift to bring the most prominent UV resonance lines (e.g., CIVλ1549, MgIIλ2800) into the visible spectrum. *IUE* ($\sim$ 1978) and *HST* ($\sim$ 1990) made it possible to observe the UV rest frame in low z AGNs resulting in the identification of several low z sources showing BALs and mini-BALs (Turnshek et al. 1988; Boroson & Meyers 1992; Barlow et al. 1997; Jannuzi et al. 1998).

One advantage of low redshift sources involves the possibility of a reliable determination of the quasar rest frame from optical emission lines or, in a few cases, host galaxy measures. An accuracy $\Delta z \lesssim 0.001$ can be achieved from [OIII]λ5007 or the peak of the narrow component of Hβ.

Another advantage stems from our ability to interpret the sources in the context of the Eigenvector 1 (E1) parameter space (Sulentic et al. 2000b). E1 tells us that AGN optical and UV emission line phenomenology is not randomly dispersed around an "average" spectrum. We identified four parameters that provide optimal discrimination between the various classes of broad line emitting AGNs. The three emission line parameters are : (1) FWHM of the Hβ broad component (H$\beta_{\rm BC}$), (2) $R_{\rm FeII}$= W(FeII λ4570)/W(H$\beta_{\rm BC}$), and (3) C(1/2) = profile centroid displacement of CIVλ1549 at half maximum. They are supplemented by (4) $\Gamma_{\rm soft}$, the soft X-ray photon index. If we think of E1 as an H-R diagram for quasars then we find a principal occupation or main sequence for the majority of low redshift sources. The sequence ranges from radio-quiet (RQ) narrow line Seyfert 1 (NLSy1) sources with narrowest FWHM(H$\beta_{\rm BC}$), strongest $R_{\rm FeII}$, largest CIVλ1549 blueshift and strongest soft X-ray excess to lobe-dominated radio-loud (RL) sources with the broadest H$\beta_{\rm BC}$ profiles, weakest $R_{\rm FeII}$ and no soft X-ray excess or CIVλ1549 blueshift. The main E1 occupation/correlation sequence is likely to be driven by the Eddington ratio (Marziani et al. 2001; Boroson 2002; Zamanov & Marziani 2002; Yuang & Wills 2003). The soft X-ray excess parameter has also been interpreted in the same scenario with the sources accreting at highest $L_{\rm bol}/M_{\rm BH}$ showing the largest values of $\Gamma_{\rm soft}$ (Pounds, Done, & Osborne 1995).

Another way to emphasize phenomenological differences in the E1 parameter space is through the Population A–B concept. Population A is an almost pure RQ population (with NLSy1 as the extremum) defined by the criterion FWHM(H$\beta_{\rm BC}$) $\lesssim$ 4000 km s^{-1} (at low z; see Sulentic et al. 2004). Population B is a mixed RL and RQ population with broader H$\beta_{\rm BC}$. Type 1 AGN show some evidence for a discontinuity between Pop. A and B in H$\beta_{\rm BC}$, CIV$\lambda1549_{\rm BC}$ profiles and occurrence of HIL blueshifts (Marziani et al. 2003c; Bachev et al. 2004). Analysis of the optical E1 parameters supports the idea that Pop. A sources are radiating at higher Eddington ratio than Pop. B (Boroson & Green 1992; Pounds et al. 1995; Marziani et al. 2003b). Further support comes from CIVλ1549 and other UV HIL resonance lines which show evidence for a wind or outflow in Pop. A sources.

2. SAMPLE DEFINITION

Defining a large, complete sample of low z BAL QSOs is impossible with present data. We select BAL + mini-BAL (BALnicity index $\approx$ 0 km s^{-1}; Weymann et al. 1991) QSOs using the following two criteria: (1) FWHM(CIV$\lambda1549)_{\rm abs} \gtrsim$ 2000 km s^{-1}, (2) and W(CIV$\lambda1549)_{\rm abs} \gtrsim$ 4 Å. This results in negligible overlap with high and low z NAL samples (e.g., Richards et al. 1999; Brandt et al. 2000; Ganguly et al. 2001; Vestergaard 2003). We consider objects with magnitude $m_{\rm V} \lesssim 16.3$ and redshift $z \lesssim 0.5$ and find 12 sources which include: (a) AGNs identified in NED as BAL QSOs (with the exception of PG 1416−129 which does not show absorption in *HST* spectra; see Green et al. 1997), (b) BAL QSOs in Turnshek et al. (1997) selected on the

TABLE 1

OBJECT IDENTIFICATION AND OPTICAL OBSERVATIONS

IAU Name (1)	Object Name (2)	m_V (3)	z (4)	M_V (5)	Date (6)	UT (7)	ET (8)	Obs. (9)
J00457+0410	PG 0043+039	16.0	0.3850 ± 0.0010	−24.84	09/10/1994	02:27	6000	ESO
J08045+6459	IRAS 07598+6508	14.31	0.1488[a] ± 0.0001	−24.42	22/02/1991	02:18	2500	KPNO
J10043+0513	PG 1001+054	16.21	0.1610 ± 0.0010	−22.77	19/02/1991	06:52	3600	KPNO
J10074+1248	PG 1004+130	15.24	0.240[b] ± 0.001	−24.57	21/04/1990	05:10	3600	BG
J11292−0424	PG 1126-041	14.69	0.0560 ± 0.0001	−22.00	19/02/1991	08:16	1800	KPNO
J12562+5652	Mrk 231	13.60	0.0412[c] ± 0.0001	−22.39	09/12/1994	09:14	3000	SPM
J13532+6345	PG 1351+640	14.3	0.0822[d]± 0.0001	−23.26	19/02/1991	10:38	1800	KPNO
J14138+4400	PG 1411+442	14.65	0.0896[d] ± 0.0005	−23.03	19/02/1991	12:31	1800	KPNO
J15366+5433	Mrk 486	14.8	0.0389[e] ± 0.0001	−20.68	01/07/1995	05:50	2400	SPM
J15547+0822	PG 1552+085	16.3	0.119[f] ± 0.001	−22.03	17/02/1990	12:17	2400	BG
J17014+5149	PG 1700+518	14.98	0.2899± 0.0007	−25.24	30/04/1995	00:13	3600	CA
J17014+5149	···	···	···	···	28/06/1995	07:27	3600	SPM
J21148+0607	PG 2112+059	15.8	0.46005± 0.00010	−25.45	18/10/1990	01:43	2400	KPNO
J21148+0607	···	···	···	···	29/06/1995	08:29	3600	SPM

[a] Solomon et al. (1997) H I 21 cm; optical determination suggests larger uncertainty (shifted by −300 km s^{-1}).
[b]Wills et al. 1999. [c]Average value of Falco et al. (1999) and de Vaucouleurs et al. (1991) (RC3).
[d]Marziani et al. (1996). [e]SIMBAD. [f]Schmidt & Green (1983).

basis of weak [O III]λ4959,5007 emission (4 objects), (c) soft X-ray weak PG QSOs with W(C IVλ1549) $\gtrsim$ 5 Å from Brandt et al. (2000), with the exception of PG 1126−041. We also visually inspected the *HST*-FOS archival spectra that included C IVλ1549 (as retrieved by Bachev et al. 2004) and found no additional sources satisfying our selection criteria.

Our conditions are less restrictive than those of Weymann et al. (1991) since we consider BAL sources with shallow absorption troughs and with FWHM(C IVλ1549)$_{\rm abs} \gtrsim$ 2000 km s^{-1}: Weymann et al. (1991) exclude sources with absorption troughs $\lesssim$ 10% of the adjacent continuum. We do not consider as BAL quasar sources with absorption of any depth but with width $\lesssim$ 2000 km s^{-1} (notable examples include Akn 564 and IRAS 04505–2958; Bechtold et al. 2002; Crenshaw et al. 2002).

Table 1 identifies the objects in our sample (Col. 1: IAU code; Col. 2: common name), and provides the apparent visual magnitude (Col. 3; the objects reported with two decimal digits are new observations; see § 3.1), the absolute V magnitude (assuming $H_0 = 75$ km s^{-1} Mpc^{-1}, $\Omega_{\rm M} = 0.3$, and $\Omega_\Lambda = 0.7$; Col. 5), the heliocentric redshift and its associated uncertainty (Col. 4; see also the beginning of § 4), the date of optical spectroscopic observations (Col. 6), the universal time at the beginning of the exposure (Col. 7) and the exposure time in seconds (Col. 8). The last column (Col. 9) provides the acronym of the observatory where the data have been collected. We use the term "low z QSOs" for all of our objects even if a few objects are at or below the formal boundary between Seyferts and QSOs ($M_{\rm B} \approx -22.1$).

3. OBSERVATIONS AND DATA ANALYSIS

3.1. *Observations*

Optical Photometric Observations B, V, Rc, and Ic observations have been obtained (16 and 17/02/2001) with the 2.0 m RC telescope of the Bulgarian National Astronomical Observatory "Rozhen", equipped with a Photometrics 1024×1024 CCD camera. Landolt (1992) standards were observed before and after every source. Apparent V magnitudes are given in Table 1. The error of our magnitudes is ±0.05 mag in all bands.

Optical Spectroscopic Observations Data used in the present study are part of a large sample of spectroscopic observations covering the Hβ spectral region (Marziani et al. 2003a). The dataset covers 215 AGNs with resolution typically around 4 Å FWHM and S/N (in the continuum near Hβ) usually $\gtrsim$ 20. Data on individual observations used in this paper are reported in Table 1.

TABLE 2

LOG OF UV ARCHIVE OBSERVATIONS

IAU Name	UV Obs.					
	Camera	Grating	Date	UT	ET (s)	Data Set
(1)	(2)	(3)	(4)	(5)	(6)	(7)
J00457+0410	*HST*/FOS	G190H/BL	28/10/1991	04:36	1315	Y0RV0204T
J08045+6459	*HST*/STIS	G140L	10/12/1998	16:37	2570	O4YY18010
	IUE/SWP	Low disp.	28/09/1989	03:38	12840	SWP37199
	IUE/SWP	Low disp.	17/12/1990	18:54	13200	SWP40376
J10043+0513	*HST*/FOS	G190H/RD	16/01/1997	00:03	1260	Y38O0208T
	HST/FOS	G190H/RD	26/12/1996	17:27	530	Y33S0304T
J10074+1248	*IUE*/SWP	Low disp.	12/01/1986	08:30	19000	SWP27517
	HST/STIS	G140M	23/03/2003	03:23	2899	O65EW03020
J11292−0424	*IUE*/SWP	Low disp.	05/01/1985	12:05	9900	SWP53285
	IUE/SWP	Low disp.	01/06/1992	07:31	5400	SWP44822
	IUE/SWP	Low disp.	01/06/1992	12:19	6600	SWP44823
J12562+5652	*HST*/FOS	G150L/BL	21/11/1996	08:40	770	Y3GS0404T
J13532+6345	*HST*/FOS	G190H/BL	05/09/1991	10:41	1500	Y0P80306T
J14138+4400	*HST*/STIS	G230L	12/02/2001	01:23	1200	O65617010
J15366+5433	*HST*/FOS	G190H/BL	15/11/1993	02:56	1440	Y1EL0302T
	IUE/SWP	Low disp.	07/05/1984	00:23	51600	SWP22932
J15547+0822	*IUE*/SWP	Low disp.	28/04/1986	13:40	10200	SWP28237
	HST/STIS	G230L	05/07/2003	07:23	900	O6MZ4I010
J17014+5149	*HST*/STIS	G230L	30/01/2001	16:27	1200	O65619010
J21148+0607	*HST*/FOS	G190H/RD	19/09/1992	14:27	2372	Y10G0204T
	HST/FOS	G270H/RD	19/09/1992	16:07	1690	Y10G0205T

UV Spectroscopic Observations UV observations are *HST*/FOS with high resolution grating (yielding a precision of $\approx$ 200 km s^{-1}), and STIS medium-resolution spectra covering C IVλ1549. FOS data were re-calibrated with the latest STPOA processing scripts using IRAF/SDAS. This takes into account systematic errors in the wavelength scale of the FOS/BL data which were not properly considered until recently (e.g., Kerber & Rosa 2000). Several *IUE* observations were also included with correspondingly lower precision $\Delta v_r \sim 1000$ km s^{-1}. In the case of Mrk 231 *IUE* data were included because only a G150L *HST*/FOS observation was usable. Table 2 provides a log of the UV archival observations employed in the present paper. Column 2 lists the telescope and the camera; Col. 3 the grating. Cols. 4, 5, and 6 provide date, universal time and exposure time respectively. Column 7 identifies the data-set.

3.2. *Optical and UV Data Analysis: Fe*II$_{\rm opt}$ *and Fe*II$_{\rm UV}$ *Emission*

Optical and UV observations were analyzed following Marziani et al. (1996; 2003c, Hβ, and C IV) and Sulentic, Marziani, & Dultzin-Hacyan (2002a). The wavelength and flux-calibrated spectra were shifted to the rest frame and then continuum and Fe II subtracted. Fe II subtraction used a scaled and broadened template based on observations of Fe II strong I Zw 1. It is now possible to define a better template for both optical and UV Fe II emission (between 1400 Å and 1800 Å). The optical one is almost identical to the one used in Boroson & Green (1992) but is based on a higher resolution spectrum. Our Fe II$_{\rm UV}$ template comes from two post-COSTAR I Zw 1 observations, the first covering the G130H spectral range (dataset Y26C0204T —13 Feb 1994) and the second covering the G190H range (dataset

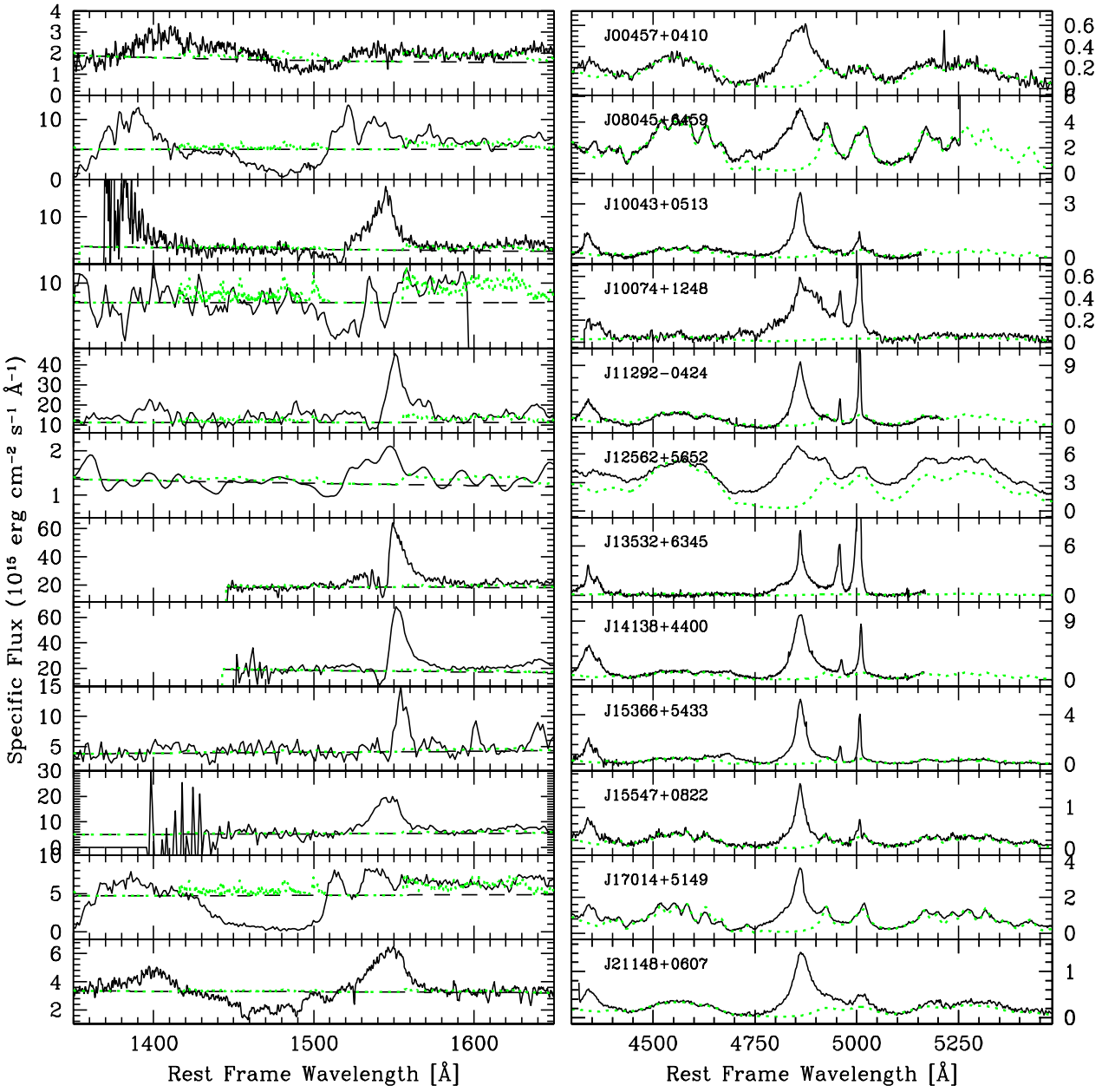

Fig. 1. De-redshifted spectra for low redshift BAL QSOs: CIVλ1549 (left) and Hβ spectral regions (right). Solid line is the spectrum converted to rest frame specific flux (ergs s^{-1} cm^{-2} Å^{-1}). Green dotted line indicate FeII$_{\rm UV}$ and FeII$_{\rm opt}$ emission. Dot-dashed lines show the continuum level.

Y26C0103T —14 Sep 1994). The template agrees with a theoretical model computed for hydrogen density $n_{\rm H}$= 10^{12} cm^{-3}, and ionizing photon density $\log \Phi_{\rm H}$=17.5 cm^{-2} s^{-1} (Verner et al. 1999). This may be the most appropriate case for the overall low ionization level observed in the spectra of NLSy1s like I Zw 1 (Marziani et al. 2001). It also agrees satisfactorily with the template of Vestergaard & Wilkes (2001). The continuum level was defined in spectral regions at $\approx$ 1450 Å and 1750 Å, where no emission features were appreciable. For three sources with strong FeII$_{\rm UV}$ emission (PG 0043+038, IRAS 07589+6508, and PG 1700+518) the final continuum level was set after FeII$_{\rm UV}$ subtraction.

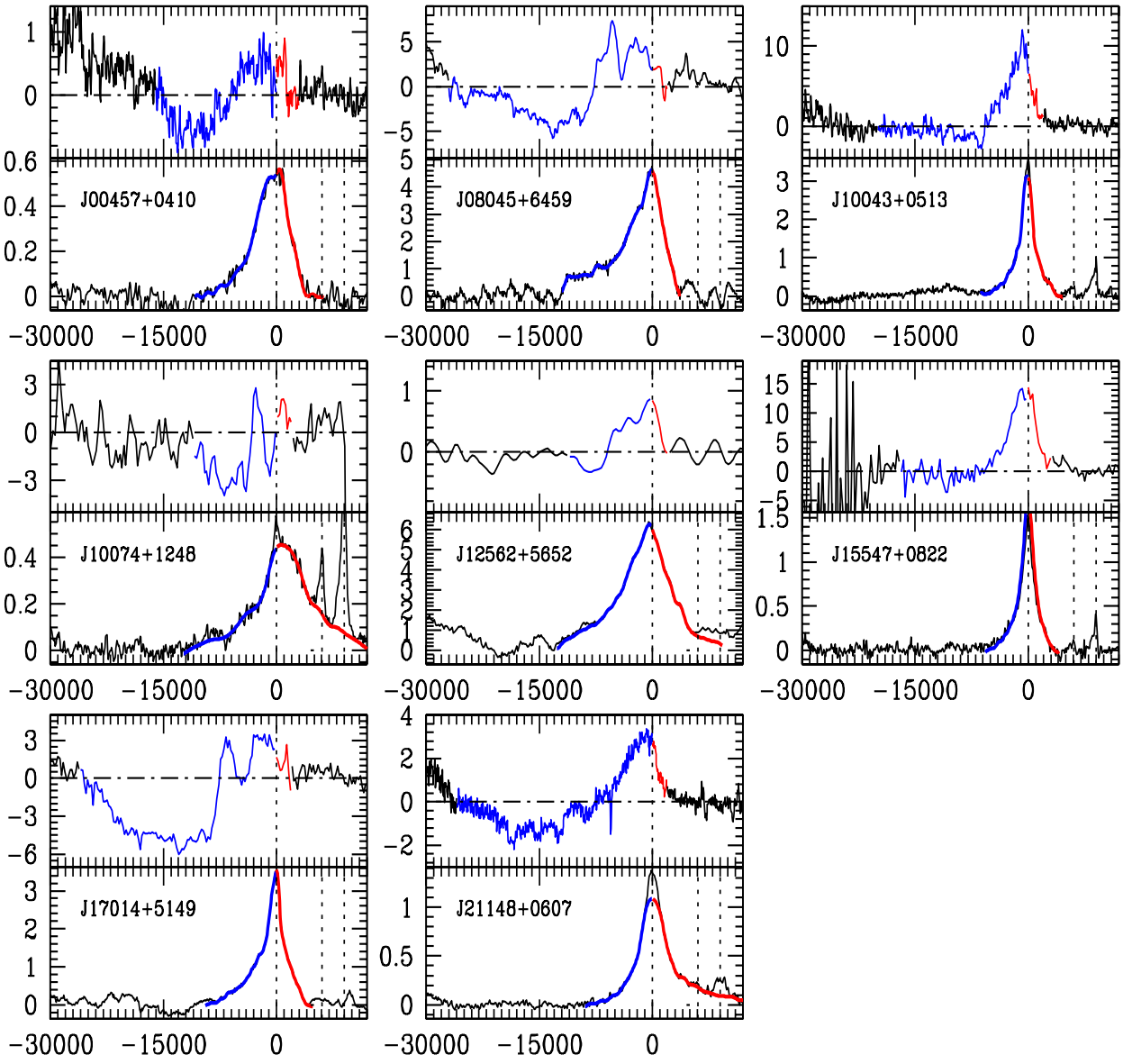

Fig. 2. Continuum and FeII subtracted profiles of CIVλ1549 and Hβ for 8 BAL QSOs in our sample. Ordinate is rest frame specific flux (10^{-15} ergs s^{-1} cm^{-2} Å^{-1}) and abscissa is radial velocity (km s^{-1}) with respect to rest frame. The upper and lower halves of each panel show CIVλ1549 and Hβ profiles respectively. A high order spline fit (thick line) superimposed on the Hβ line indicates the broad component. Dotted lines mark the quasar rest frame for CIVλ1549 and Hβ, as well as the expected position of [OIII]λ4959,5007. The sides of the absorption/emission profiles below and above $v_r \approx 0$ km s^{-1} are colored blue and red respectively.

4. RESULTS

4.1. Hβ *and* CIVλ*1549 Profile Analysis*

Rest-frame CIVλ1549 and Hβ spectral regions are shown in Figure 1 for the entire sample. The rest frame was assumed to be equivalent to the redshift of the *narrow* optical emission lines except for one source where an H I measure was available (see notes to Table 1 for refer- ences; if no reference is given then z determination was estimated in this study). We found no evidence for a signifi- cant discrepancy between [OIII]λ4959,5007 measure- ments and other narrow lines (including the peak of Hβ which was also used as an [OIII]λ5007 surrogate when [OIII]λ5007 was not detected; § 4.2.

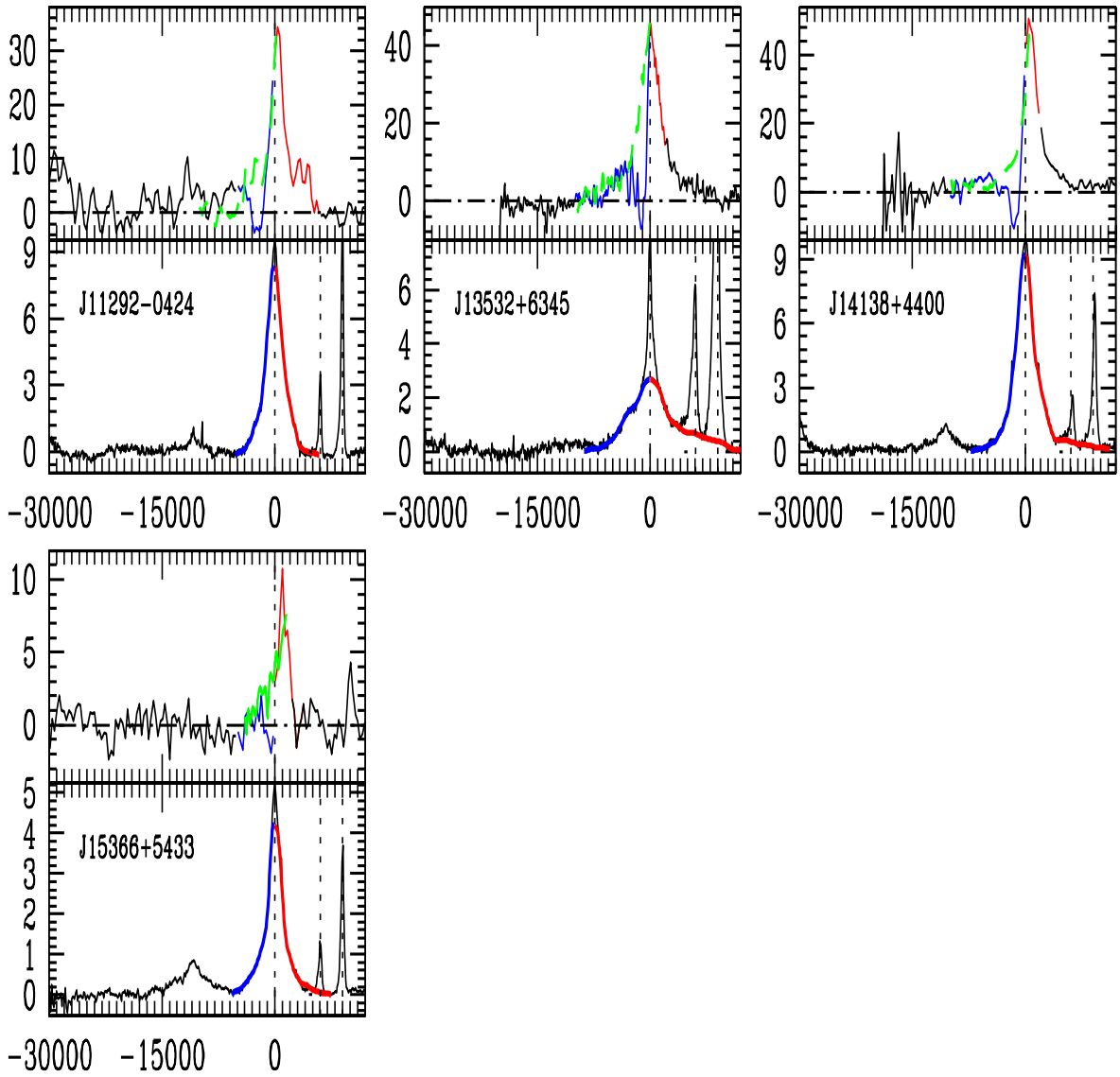

Fig. 3. Continuum and FeII subtracted profiles of CIVλ1549 and Hβ for n = 4 mini-BAL QSOs in our sample following Figure 2. Dashed line (colored green) shows the assumed unabsorbed profile used for absorption component measurements. In the case of Mrk 486 ($\equiv$ J15366+5433), the thick green line shows the *HST* CIVλ1549 profile with no absorption.

Cleaned CIVλ1549$_{\rm BC}$ and H$\beta_{\rm BC}$ profiles are shown in Figure 2 and Figure 3. The H$\beta_{\rm BC}$ profile is emphasized by a high-order spline following Marziani et al. (2003a). Table 3 lists the measured rest frame parameters for the Hβ spectral region: W(H$\beta_{\rm BC}$), R$_{\rm FeII}$, FWHM(H$\beta_{\rm BC}$), and FWHM(FeII λ4570) with uncertainty at a 2σ confidence level. Columns 2 to 4 of Table 4 list the parameters for the emission component of CIVλ1549: peak $v_{\rm r}$, equivalent width, and FWHM(CIVλ1549) after FeII$_{\rm UV}$ correction, respectively. In addition we report: radial velocity at minimum trough (Col. 5), maximum blueshift velocity of the absorption (i.e., the terminal velocity, Col. 6), the equivalent width (Col. 7), FWHM of the principal broad absorption component (Col. 8), and BALnicity index as defined by Weymann et al. (1991, Col. 9). All values are for the source rest frame. Errors in EW and FWHM are usually $\approx$ 20%. Radial velocity measurements have a similar uncertainty, unless noted. BALnicity index uncertainty is esti-

TABLE 3

$H\beta_{BC}$ AND FeII

IAU Name	W($H\beta_{BC}$) [Å]	R_{FeII}	FWHM($H\beta_{BC}$) [km s^{-1}]	FWHM(FeII λ4570) [km s^{-1}]
(1)	(2)	(3)	(4)	(5)
J00457+0410	101 ± 11	0.74 ± 0.17	4000 ± 700	4300 ± 1000
J08045+6459	77 ± 7	1.21 ± 0.19	5000 ± 400	2100 ± 300
J10043+0513	93 ± 5	0.49 ± 0.11	1900 ± 300	1850 ± 300
J10074+1248	37 ± 4	$\lesssim$0.39	6700 ± 300	···
J11292-0424	82 ± 8	0.78 ± 0.16	2300 ± 500	3100 ± 800
J12562+5652	45 ± 15	1.78 ± 0.67	6600 ± 900	$\approx$ 3000
J13532+6345	34 ± 4	$\lesssim$0.19	5900 ± 300	···
J14138+4400	86 ± 4	0.36 ± 0.09	2600 ± 200	2600 ± 500
J15366+5433	84 ± 4	0.40 ± 0.08	1800 ± 200	1850 ± 500
J15547+0822	54 ± 5	1.40 ± 0.21	2300 ± 300	···
J17014+5149	55 ± 5	0.98 ± 0.13	2200 ± 300	1700 ± 400
J21148+0607	118 ± 11	0.53 ± 0.11	3800 ± 700	4050 ± 1000

TABLE 4

CIVλ1549

IAU Name	Emission			Absorption				
	v_r [km s^{-1}]	W(CIV) [Å]	FWHM(CIV) [km s^{-1}]	v_r [km s^{-1}]	$v_{r,T}$ [km s^{-1}]	W(CIV) [Å]	FWHM(CIV) [km s^{-1}]	Baln.I. [km s^{-1}]
(1)	(2)	(3)	(4)	(5)	(6)	(7)	(8)	(9)
J00457+0410	−1800	10	8000	−11300	−16000	−11	7300	0
J08045+6459	−5000:	33:	6000:	−13400	−27000	−40	9000	5300
				−3900		−10	1160	0
J10043+0513	−1300	52	3800	−8700	−12000	−5	3000	400
J10074+1248	−3000:	3^{+2}_{-2}	6000:	−6700	−12000	−12	5950	1050
				−930		−4	1500	0
J11292−0424	$+900^{+200}_{-1000}$	42:	2200:	−2400	−5000	−4.6	1500	0
J12562+5652	$+0^{+500}_{-1000}$	16	5900	−8300	−10000	−5	3400	50
J13532+6345	+0	31:	2400	−1200	−3500	−5.5	1800	0
J14138+4400	$+300^{+200}_{-1000}$	36:	2200:	−1450	−4000	-7^{+2}_{-7}	1000^{+2000}_{-500}	0
J15366+5433	+1000	18	1500	−800	−2500	−4	1500	150
J15547+0822	-1000^{+500}_{-500}	60	3700	−11000	−17000	-6^{+2}_{-6}	5000:	500
J17014+5149	−3100:	19^{+10}_{-10}	7000:	−15000	−27000	−73	14200	10300
				−5000		−4.5	2200	0
J21148+0607	−550	23	4600	−15600	−26000	−22	9700	2500

Note to table: A double colon mark indicates highly uncertain values.

mated to be ±500 km s^{-1} at a 2σ confidence level. Some values with extremely asymmetric error bars have uncertainties indicated in the table.

Fig. 2 shows the continuum and FeII subtracted CIVλ1549 and Hβ profiles for BALs while Fig. 3 shows the spectra of the 4 mini-BALs. Fig. 3 shows

the assumed unabsorbed profile estimated by reflecting the red unabsorbed side of the emission profile onto the blue absorbed side. This procedure works especially well for PG 1351+640 and PG 1411+442 where the mini-BAL troughs appear to be displaced blueward from the peak emission. In the case of BALs we measured the absorption equivalent width by interpolating the continuum across the absorption profile.

Several characteristics are important in the context of BAL QSOs:

1. The emission component of CIVλ1549 is almost fully blueshifted relative to the rest frame velocity (e.g., Reichard et al. 2003).

2. Three out of six sources (IRAS 07598+6508, PKS 1004+13, PG 1700+518) with BALnicity Index $\gtrsim 0$ km s^{-1} show a secondary absorption trough with variable velocity ($v_{\rm r}$) relative to the rest frame from source to source, but located close to the average radial velocity of the emission component. Secondary absorptions are not easily attributed to a line-locking interpretation. The absorption velocity may correlate with the terminal velocity of the BAL: two sources with $v_{\rm r,T} \sim 27,000$ km s^{-1} have $v_{\rm r,sec} \approx$ 4000 km s^{-1}, while if $v_{\rm r,T} \sim 15,000$ km s^{-1}, $v_{\rm r,sec} \sim 1000$ km s^{-1}. The secondary component is apparently not rare, or restricted to our sources. Approximately 30% of the CIVλ1549 absorption/emission profiles in Korista et al. (1993) include a secondary absorption and appear similar to ours. About 50% of sources show a complex absorption pattern or a PHL 5200-like profile, where the CIVλ1549 emission component appears as a spiky feature because it is almost completely eaten away by deep and very broad absorption (Turnshek et al. 1988). This kind of feature does not seem to be present in the remaining $\approx 20\%$ of BAL sources.

3. The depth of the associated secondary absorption component suggests a covering factor $0.5 \lesssim f_{\rm c} \lesssim 1$.

4. BAL absorption apparently affects only a minor part of the emission component since spectral type A3 (the most extreme Pop A/NLSy1 subtype in Sulentic et al. (2002) —see Figure 4 in that paper) shows CIV$\lambda1549_{\rm BC}$ emission FWHM$\lesssim 5000$ km s^{-1} consistent with the width of CIVλ1549 emission in unabsorbed sources.

Individual sources merit a few additional comments which are given in Appendix A.

4.2. *BAL QSOs in the E1 Parameter Space*

BAL AGN with terminal wind velocities in the range $\approx$ 20,000–30,000 km s^{-1} are either outliers or are located along the upper part of the E1 "main sequence" for Pop. A sources (Fig. 4) with a possibly different distribution than the unabsorbed quasar distribution (as shown by Sulentic et al. 2002) and also from that of the mini-BAL AGN. The two sources that are located far from the "main sequence" and related model grid are hypothesized to be very rare because few quasars of any kind are found in that region (see § 4.2.1).

The upper edge of the E1 "main sequence" has been modelled as the domain of sources more highly inclined to our line of sight (i.e., with the accretion disk seen more edge-on). The grid of $L_{\rm bol}/M_{\rm BH}$ and orientation angle values superposed on the optical E1 plane in Fig. 4 was computed for a fixed value of $M_{\rm BH} \approx 10^8\ M_\odot$ (as in Marziani et al. 2001). This $M_{\rm BH}$ value is used because the average virial $M_{\rm BH}$ for our source sample is $\log M \approx 8.1$ in solar units (following Marziani et al. 2003b; Sulentic et al. 2005). There seems to be no correlation with black hole mass. The dependence on mass in the E1 diagram is rather weak, and the dispersion of $\log M \approx 0.6$ is less than the mass difference needed to have effects comparable to the ones due to orientation ($\Delta \log M \approx 1$, at least). However, sources with larger $M_{\rm BH}$ also tend to be displaced upwards (i.e., toward larger FWHM(H$\beta_{\rm BC}$); Zamanov & Marziani 2002). The location of the BAL QSOs in the optical E1 plane can be considered only as suggestive of larger inclination.

An orientation indicator appears to be emerging for the RQ Pop. A quasars as a low inclination blue outlier source population (showing a significant [OIII]λ4959,5007 blueshift: Zamanov et al. 2002; Marziani et al. 2003b). Blueshifts of several hundred km s^{-1} are observed in [OIII]λ4959,5007 for some NLSy1 (extreme E1 Pop. A sources), especially in sources with unusually weak [OIII]λ4959,5007 (Zamanov et al. 2002; Marziani et al. 2003b). Blue outliers may involve the youngest type 1 sources (Sanders et al. 1988; Zamanov et al. 2002). None of the 12 blue outliers with available UV data show BAL properties, suggesting that BALs are not observed pole-on. The mini-BAL phenomenon appears to occur over a wider range of inclination angles if our small sample can be taken as indicative. It is worth noting that NAL sources show no occupation restriction in E1 —they are found everywhere.

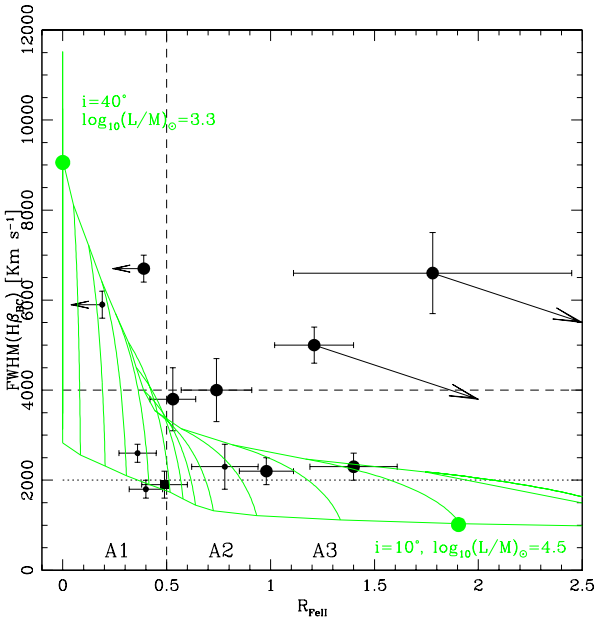

Fig. 4. The optical parameter plane of Eigenvector 1 with our sample BAL and mini-BAL quasars indicated by large and small dots, respectively. Small and large dashed horizontal lines indicate upper limits for NLSy1 and Pop. A sources. The green continuous line traces the expected location as a function Eddington ratio and orientation, following Marziani et al. (2001). The grid represents the principal zone of low z source occupation as modelled for an $M_{\rm BH}$= 10^8 $M_\odot$. The large, circular dots set the scale of the grid indicating the expected position for $i = 40^\circ$ and log $L_{\rm bol}/M_{\rm BH}\approx$ 3.3 (in solar units; upper right) and for $i = 10^\circ$ and log $L_{\rm bol}/M_{\rm BH}\approx$ 4.5 (lower left). Lines tracing the orientation effect between minimum and maximum i are incremented by $\Delta \log L_{\rm bol}/M_{\rm BH} = 0.1$. Arrows on outlier sources (Mrk 231 and IRAS 07598+6508) indicate direction of displacement after correction for a wind-related Hβ component not seen in most other low $-z$ quasars. The square identifies PG 1001+054 which has a highly uncertain absorption trough.

4.2.1. *E1 Outliers: Mrk 231 and IRAS 07598+6508*

We first point out that FWHM(H$\beta_{\rm BC}$)$\approx$ FWHM(FeII$_{\rm opt}$) within the uncertainty for all/most pop. A sources in our sample of $\approx$ 300 low z AGN Marziani et al. (2003b). The only two convincing exceptions are Mrk 231 and IRAS 07598+6508. Our E1 sample studies suggest that H$\beta_{\rm BC}$ in Pop. A sources can usually be modeled with a symmetric Lorentzian function (Sulentic et al. 2002). Fig. 2 shows that Mrk 231, IRAS 07598, and perhaps a few other sources, show a blue asymmetric Hβ profile that could be modeled as a separate strongly blueshifted component. The presence/absence of this extra component will affect FWHM measures for H$\beta_{\rm BC}$ (Figure 5). If one considers only the unshifted component with width comparable to FWHM(FeII$_{\rm opt}$) then the two sources move into the region with FWHM(H$\beta_{\rm BC}$)$\lesssim$ 4000 km s^{-1}. These two sources are among the strongest FeII$_{\rm opt}$ emitters in our sample. If we consider only the FeII-like Lorentzian component of H$\beta_{\rm BC}$ in deriving the R$_{\rm FeII}$ parameter we find a large increase to $\approx$ 5 and 3 for Mrk 231 and IRAS 07589+6508 respectively. If they are now compared to the rest of the sample they will show the largest values of R$_{\rm FeII}$ and will lie close to the upper FWHM boundary for NLSy1s. The blueshifted line component roughly corresponds to the blueshifted C IVλ1549 emission component, and it is not unreasonable to argue that part of the Balmer emission could arise in the postulated wind/outflow where most of the C IVλ1549 is produced. Alternatively, the blueshifted H$\beta_{\rm BC}$ residual could be associated to a nuclear starburst. A similar interpretation is possible for PG 0043+039 although the blueward asymmetry in the H$\beta_{\rm BC}$ profile is below half maximum.

4.3. *A Terminal Velocity-Luminosity Correlation?*

Four out of five BAL QSOs with highest terminal velocities ($v_{\rm T} \lesssim 15,000$ km s^{-1}) are Pop. A sources which have higher $L/L_{\rm Edd}$ in general (Marziani et al. 2003b). Indeed, in our sample we find evidence for a correlation between terminal wind velocity and absolute V magnitude (Figure 6). This is expected if the Eddington ratio is governing the wind/outflow as, for example, in the case of radiation pressure driven

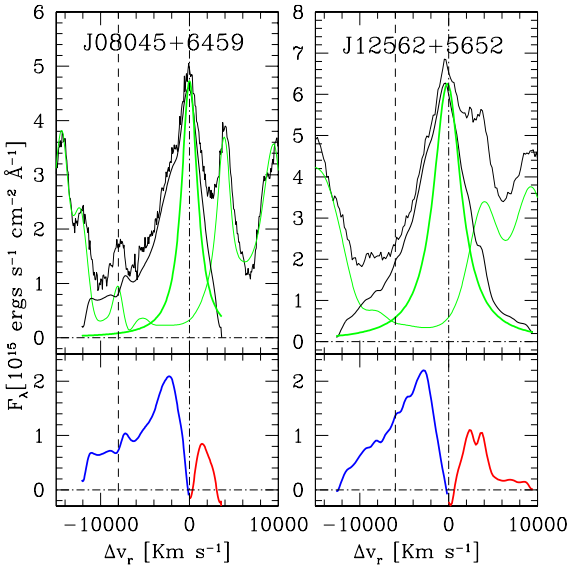

Fig. 5. Outlier sources IRAS 07598+6508 (≡ J08045+5459, left) and Mrk 231 (≡ J12562+5652, right) H$\beta_{\rm BC}$ with Lorentzian profile model of unshifted component most similar to majority of sources (thick green line) using same width Fe II$_{\rm opt}$ lines (≈ 2100 km s^{-1}; thin green lines). Original continuum subtracted spectra shown as thin solid lines. Thick solid lines show "cleaned" H$\beta_{\rm BC}$ (after Fe II$_{\rm opt}$ subtraction). Lower panel: Residual components after subtraction of the Lorentzian profile from H$\beta_{\rm BC}$. Dashed line marks the radial velocity at which C IVλ1549 absorption begins. Abscissa is radial velocity difference from rest frame (km s^{-1}); ordinate is rest frame specific flux.

winds (Laor & Brandt 2002).

The highest terminal velocities are likely possible only for Pop. A objects where we see the blueshifted C IVλ1549 emission component. However the conclusion that BAL QSOs are exclusive to Pop. A is challenged by the discovery of radio-loud BAL QSOs in the FIRST survey (Becker et al. 2000) as well as by the presence in our sample of the Pop. B source PKS 1004+13 (FWHM(H$\beta_{\rm BC}$)≈ 7000 km s^{-1}) that was identified as the first radio-loud BAL QSO relatively recently (Wills, Brandt, & Laor 1999).

The terminal velocity, in the case of a pressure driven wind, is $v_{\rm T} \propto \sqrt{L/L_{\rm Edd}}$. Considering the classical BAL QSOs in our sample, we have

$$v_{\rm T} \approx \frac{\rm FWHM(CIV)}{2} \sqrt{f_{\rm M} \frac{L}{L_{\rm Edd}}}\,,$$

(cf. Laor & Brandt 2002). If we assume that the force multiplier $f_{\rm M}$ is a function of ionization parameter U (defined as the ratio of the photon density to electron density), well approximated by $f_{\rm M} \approx 10^{2.55} U^{-\frac{1}{2}}$ (Arav, Li, & Begelman 1994), we can write the terminal velocity as

$$v_{\rm T} \approx 10^4 \ {\rm FWHM(CIV)}_{1000} U^{-\frac{1}{4}} (\frac{L}{L_{\rm Edd}})^{\frac{1}{2}} \ {\rm kms}^{-1},$$

where FWHM(C IVλ1549) is in units of 1000 km s^{-1}. FWHM(C IVλ1549)/2 can be taken as a rough estimate of the initial injection velocity in the case of a radial flow. If we assume: (1) that the most extreme pop. A sources radiate close to the Eddington limit while Pop. B sources typically have $L/L_{\rm Edd} \approx 0.1$, and (2) that a proper FWHM(C IVλ1549) value is 4000 km s^{-1} and 6000 km s^{-1} for Pop. A and B, respectively, we find $v_{\rm T} \sim 40,000\ U^{-1/4}$ km s^{-1} (Pop. A, $U \gtrsim 0.01$) $> 20,000\ U^{-1/4}$ km s^{-1} (Pop. B, $U \lesssim 0.5$). Simple radiation-driven wind considerations are therefore consistent with the existence of a Pop. B BAL source and are predicting systematically lower $v_{\rm T}$, as implied by the observations. The terminal velocity in RL BAL QSOs may also be systematically lower than in RQ BAL QSOs (Becker et al. 2000) as is true for our single example. Therefore, a Pop. B source does not necessarily undermine the idea of a critical Eddington ratio accounting for the Pop. A–B dichotomy.

At this point in time the evidence suggests that RL or RQ Pop. B BAL sources are rare. The NLSy1-like properties (FWHM(H$\beta_{\rm BC}$)≈ 2100 km s^{-1} and strong Fe II$_{\rm opt}$) of J1556+3517 motivated our skepticism about the RL designation for this source (Becker et al. 1997). It is now known that it probably suffers from strong optical extinction (Najita, Dey, & Brotherton 2000) and is RQ. This warrants caution

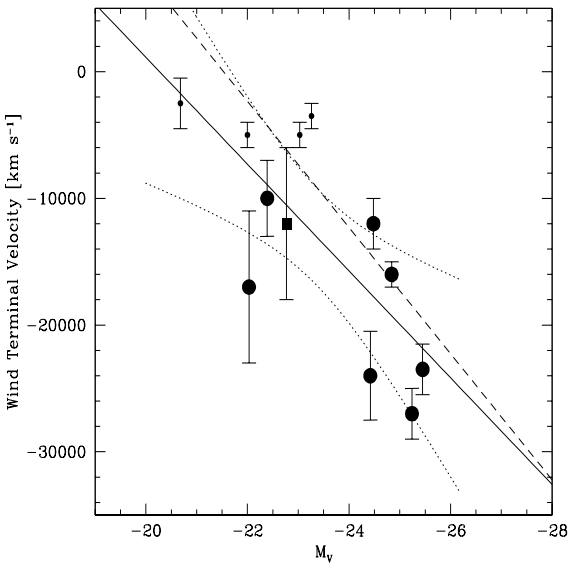

Fig. 6. Correlation between absolute V magnitude M_V and wind terminal velocity (in km s^{-1}). Symbols used for data points have the same meaning of Fig. 4. The solid line is an unweighted least-squares fit made including all 12 data points. The dotted lines trace the ±95% confidence intervals. The dashed line is the fit shown in Fig. 6 of (Laor & Brandt 2002), converted to the cosmology adopted in this paper.

about other claimed RL BALs especially if they show Pop. A characteristics (see Brotherton et al. 1998; Sulentic et al. 2004). PKS 1004+13 is a genuine RL Pop B source, and unless many more are found, one should consider it as a rare RL BAL source.

5. DISCUSSION

5.1. *A Simple Model for Interpretation of the* CIVλ*1549 Profiles*

Our results, coupled with the main constraints set by much earlier work (see reviews by Turnshek 1986; Crenshaw et al. 2003), lead to a simple geometrical and kinematical model (Figure 7). We ascribe the high-ionization line emitting BLR to a wind as is now widely accepted. An immediate inference from *a fully blueshifted* emission component involves a radial flow ($v/v_{\rm rot} \gg 1$) with an opening angle $\lesssim 90°$ if BALQSOs are those QSOs viewed near the maximum possible orientation ($i \sim 45°$). The BAL region might extend in a conical corona of divergence angle $\lesssim 10°$ (which would include our line of sight; Fig. 7). The absorption profiles are furthermore consistent with a radiation driven wind launched at *roughly* the outer radius of the BLR because the emission component is only marginally "eaten away" by the BAL. This appears to be the case for the sources in this paper as well as for many BAL QSOs in high–z samples (e.g., Korista et al. 1993).

While this scheme is fully consistent with a "standard BAL QSO model" that has emerged over the course of more than 15 years of research, the observation of secondary absorption components may require an additional element. We suggest that whenever a secondary absorption is present we may be observing an axial region covering all of the continuum-emitting region and part of the BLR as well. This property is needed to explain the depth of the absorption which implies $f_c \gtrsim 0.5$. This axial region may involve a cylindrical sheet of absorbing gas with different physical properties than the BAL region. However, it appears to share the BLR flow because the absorption is located close to the center of the CIVλ1549 emission component in all three cases presented here. The narrower absorption profile may result from a restricted viewing angle $\approx 50°$. It is important to stress that a shell of absorbing material which could provide an adequate f_c is not viable in the geometrical context of our model because of the relatively narrow absorption. A flow spiralling outward i.e., with a significant rotational component may also produce the secondary absorption although it seems again difficult to explain the absorption depth.

The cylindrical sheet may have a straightforward physical explanation if it is connected with axial flows. A two-fluid model for relativistic outflows includes a fast relativistic beam surrounded by

TABLE 5

HIGH–Z BAL OR MINI-BAL QSOs WITH CIVλ1549 SHIFT[a]

Object	z	FWHM(Hβ) [km s^{-1}]	FeII$_{\rm opt}$	[OIII]	$\Delta v_{\rm r}$ (CIVλ1549) [km s^{-1}]
(1)	(2)	(3)	(4)	(5)	(6)
0043+008(UM275)	2.146[b]	4300:	weak	mod.	0[c]
	2.1526[d]				−500[c]
0226−038 (RL?)	2.073[b]	2800:	weak	strong	−900[e]
0842+345(CSO203)	2.163[b]	8400:	strong	weak	−3000[c]
1011+091	2.305[b]	7500:	strong	weak	−4000[c]
1246−057	2.244[f]	4500[g]	strong	weak	−2000[c]
	2.243[b]	5900:	strong	weak	−2000[c]
	2.246[h]				−2200[c]
1309−056	2.220[b]	3200:	strong	weak	−750[c]
	2.239[h]				−2500[c]
H1413+117	2.551[f]	4000[g]	strong	strong	0[j]
	2.558[i]				−600[j]
LBQS2212−1759	2.228[b]	6100:	weak	strong	−600[c]

[a]Sources for which a reliable measurements of systemic z and CIVλ1549 emission component shift exist.

[b]From [OIII]λ4959,5007 as reported in McIntosh et al. (1999).

[c]Korista et al. (1993) UV/CIVλ1549 redshifts. [d]From SDSS. [e]UV z from Lanzeta, Wolfe, & Turnshek (1987). [f] Hill, Thompson, & Elston (1993). [g]Hill et al. (1993) – Hα. [h]Espey et al. (1989) – Hα.

[i]Barvainis et al. (1997) from CO. [j] CIVλ1549 emission; Angonin et al. (1990).

a slower, possibly thermal, outflow with a mixing layer between the beam and the jet (e.g., Lobanov & Roland 2004). A black hole with specific angular momentum significantly different from zero, or even approaching the maximally rotating case ($a/M \approx 0.998$), is required for driving relativistic, radio-emitting jets (Blandford & Znajek 1977). The most straightforward evidence for black holes with $a/M \gtrsim 0$, apart from the existence of radio jets, comes from Fe Kα profile shape and variations in a RQ Pop. A source, MCG –06–30–15 (Sulentic et al. 1998), as well as from energy considerations for rapidly-varying X-ray sources (Forster & Halpern 1996) which are again RQ Pop. A sources. In a scenario where some NLSy1s and, at least, some other Pop. A sources are young/rejuvenated quasars (Mathur 2000; Sulentic et al. 2000a), they may have experienced one of the rare accretion events leading to a consistent increase of the black hole angular momentum (unlike mass, black hole angular momentum can reverse and decrease through BH mergings and accretion; Gammie et al. 2004; Hughes & Blandford 2003). Accretion events leading to refueling of the central BH are expected to be driven by mergers or strong interactions between galaxies. These give rise to an enhancement in FIR emission (observationally) thought to reflect enhanced star formation activity (physically; Canalizo & Stockton 2002; Lípari et al. 2004, and references therein). Three sources in our sample are Ultra-Luminous IR sources ($\log L_{\rm FIR} \gtrsim 12$ in solar units). They are the two E1 outliers as well as PG 1700+518. It is interesting to note that, on the basis of the $L_{\rm bol}/M_{\rm BH}$ dependence shown in Fig. 4, the observed $R_{\rm FeII}$ for Mrk 231 and IRAS 07598+6508 would require highly super-Eddington accretion unless the accreting object is a Kerr black hole. The only radio loud source in our sample of BAL QSOs (PKS 1004+13) is one of the 3 sources with a deep secondary absorption. As a final speculation, we therefore suggest that the inner cylinder may be observed only in sources whose central black hole has a significant spin.

The proposed axial sheet of gas is actually a variant of the model proposed by Elvis (2000) to explain the occurrence of BAL and NAL. Bent flow lines seen at large viewing angles, or along the flow, could give rise to NAL and BAL, respectively. This would require that the flow be observable at large inclinations ($i \rightarrow 90^{\circ}$) which is not supported by the properties of the CIVλ1549 profiles in our sample.

5.2. *From Low z to High z BAL QSOs*

It is interesting to consider the CIVλ1549 emission properties of the few high–z BAL QSOs for which a rest frame can be determined. Table 5 lists all cases that could be found in the literature. Following the source name and redshift we list: FWHM(H$\beta_{\rm BC}$) (Col. 3), qualitative evaluations of the strengths of FeII$_{\rm opt}$ and [OIII]λ4959,5007, respectively (Cols. 4 to 5), as well as radial velocity shift of the CIVλ1549 emission component with respect to the rest frame (Col. 6, references are given in the footnotes). FWHM(H$\beta_{\rm BC}$) and $\Delta v_{\rm r}$ are given in the quasar rest frame. We see that CIV$\lambda1549_{\rm BC}$ is most often shifted by $\gtrsim$ 1000 km s^{-1}and overall the properties are more consistent with Pop. A than Pop. B sources. This provides some support for the assumption that our sources are low redshift analogues of the larger high redshift BAL population, even if our small sample cannot sample all of the rich high–z BAL QSO phenomenology. High–z BAL QSOs studied by Hartig & Baldwin (1986) show large SiIII]λ1892/CIII]λ1909, strong FeII$_{\rm UV}$, low W(CIVλ1549) in emission and large blueshifts with respect to MgIIλ2800. These are also typical properties of Pop. A sources (Zamanov et al. 2002; Bachev et al. 2004).

5.3. *BAL QSOs and the General QSO Population*

The model sketched in Fig. 7 also helps us to understand the relationship between BAL QSOs and general Pop. A of quasars. Blueshifted CIVλ1549 emission profiles have been known for a long time (Gaskell 1982) and, at low z, the most extreme examples are observed in prototype NLSy1 sources like I Zw 1. Systematic CIVλ1549 blueshifts are also observed in the larger domain of Population A sources that include NLSy1s (Sulentic et al. 2000b). The HIL CIVλ1549 properties (and corresponding LIL H$\beta_{\rm BC}$ properties) were interpreted as arising in a HIL wind (from a LIL emitting accretion disk; Marziani et al. 1996; Dultzin-Hacyan et al. 2000). If a source is observed almost pole-on the outflow gives rise to a fully blueshifted CIV$\lambda1549_{\rm BC}$ profile. At the same time we observe the narrowest H$\beta_{\rm BC}$ profiles implying that the outflow has a major velocity component perpendicular to the disk (for a fixed $L_{\rm bol}/M_{\rm BH}$; Marziani et al. 2001). This is consistent with the properties of e.g., I Zw 1 or Ton 28 with respect to the generality of Pop. A sources. The blueshift of CIV$\lambda1549_{\rm BC}$ is smaller if the wind system is observed at larger angles. As the inclination increases, a rotational component from the disk may further reduce the CIV$\lambda1549_{\rm BC}$ profile shift. However, since we still observe an *almost* fully blueshifted CIV$\lambda1549_{\rm BC}$ in several BAL QSOs of our sample, it seems unlikely that the inclination and the half-opening angle of the radial flow exceed $\approx 45^\circ + 10^\circ \approx 55^\circ$.

One must also take into account that $v/v_{\rm rot}$ is expected to be a function of $L_{\rm bol}/M_{\rm BH}$, and hence to increase with R$_{\rm FeII}$ (Marziani et al. 2001). This lowers the likelihood of observing a large CIV$\lambda1549_{\rm BC}$ blueshift as one goes from population A3 spectral types to B following the definition of Sulentic et al. (2002). BAL QSOs with CIVλ1549 profiles like the PG 1700+518 one are therefore most likely Pop. A sources observed at extreme Eddington ratio and at higher inclination. Their pole-on counterparts may be sources like I Zw 1.

The absence of any significant absorption at the CIV$\lambda1549_{\rm BC}$ line center may be telling us that there is no significant spin in the central engines. If black hole angular momentum is different than 0 we can expect to see the "central" absorption observed in BAL QSOs at the blue edge of the CIV$\lambda1549_{\rm BC}$ emission profile as a detached mini-BAL. Such features may be rare and of modest equivalent width.

6. CONCLUSION

This work supports the standard model for BAL QSOs (i.e., a radiation-driven wind flowing out at the edge of the BLR), which directly accounts for most of the absorption/emission line properties observed in our small low z sample. The E1 correlations allow us to ascribe the most extreme BAL phenomenology to large Eddington ratio sources, and at the same time to account for the existence of BALs in sources radiating at relatively low Eddington ratios (§§ 4.2, 4.3). In the context of the E1 scenario it also suggests an axial structure associated with vertical ejection contributing to the absorption, a suggestion requiring further testing.

This paper emphasizes the importance of having full coverage of the rest frame spectrum from 1500 Å to the Balmer lines. In this case the data allow to accurately determine the quasar rest frame and to use the E1 parameter space plus a simple geometric model to interpret new results. This approach is now becoming possible for intermediate redshift quasars ($1 \lesssim z \lesssim 2$) where IR spectra preserve access to the region of Hβ.

The authors acknowledge support from the Italian Ministry of University and Scientific and Technological Research (MURST) through grant and Cofin 00−02−004. D. D.-H. acknowledges support from grant IN100703 PAPIIT UNAM. We thank

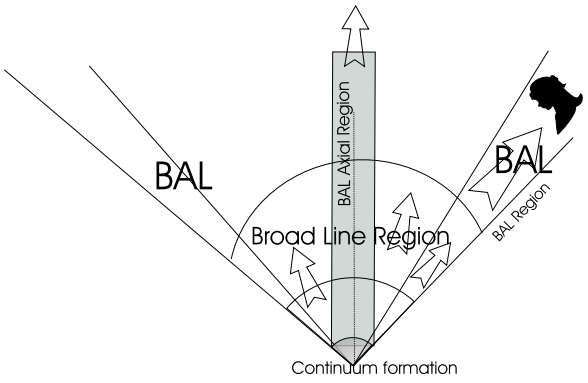

Fig. 7. Cartoon depicting the basic structure needed to account for the BAL profiles discussed in §5.1. The observer looking at the edge of a cone of opening angle $\approx 100°$, sees a fully blueshifted emission component, a BAL and a second, narrower BAL originating in an axial sheet of gas participating in the general BLR outflow. See text for details.

M.H. Ulrich for permission to use the ESO PG 0043+039 spectrum. This research has made use of the NASA/IPAC Extragalactic Database (NED) which is operated by the Jet Propulsion Laboratory, California Institute of Technology, under contract with the National Aeronautics and Space Administration.

APPENDIX A

A. Properties of Individual Sources

PG 0043+039 ≡ J00457+0410. Shows a FIR excess but only a marginal outlier in the E1 plane. The BALnicity index reported goes to 0 because of the placement of the continuum, which is likely to be more accurate in this study because of the Fe II$_{\rm UV}$ subtraction, even if the absorption trough remains evident.

IRAS 07598+6508 ≡ J08045+6459. This intriguing object shows a FIR excess, and its location in the E1 plane is peculiar. It is interesting to note that FWHM(H$\beta_{\rm BC}$) $\approx$ 5000 km s^{-1} $\gg$ FWHM(Fe II) $\approx$ 2000 km s^{-1}. The good S/N ratio and the strength of Fe II$_{\rm opt}$ emission, along with the large W(H$\beta_{\rm BC}$) make this result especially striking (see § 4.2.1 and Fig. 5).

PG 1001+054 ≡ J10043+0513. Source PG 1001+054 has a fairly uncertain absorption trough; could be a detached (or almost detached) mini-BALs. The mini-BAL interpretation is supported by the location of this source in the E1 diagram (Fig. 4). There is no evidence of spectral variability from the three spectra employed in this study.

PG 1004+130 ≡ J10074+1248. The brightest radio loud BAL QSO, recognized by Wills et al. (1999). The C IVλ1549 absorption and emission properties resemble those of the Pop. A BAL QSO with BALnicity index $\gg 0$, although this object is a lobe-dominated radio loud quasar, with FWHM(H$\beta_{\rm BC}$)$\approx$ 7000 km s^{-1}.

PG 1126−041 ≡ J11292−0424. A bona-fide mini BAL-QSO.

Mrk 231 ≡ J12562+5652. *HST*/FOS observations with grism G190H produced only noisy spectra due to the strong internal extinction. Mrk 231 is well known for the prototypical ULIRG and mixed/starburst AGN properties, and the SED shows an impressive FIR excess over the typical RQ SED. The useful spectra were taken with the low dispersion grism. The BALnicity index for C IVλ1549 is close to 0 km s^{-1}; however, this should be viewed with some care due to the heavy internal reddening ($A_{\rm V} \approx 2$; Lípari, Colina, & Macchetto (1994). Fe II emission is not well reproduced by the template, but this is more likely to be due to the heavy internal reddening rather than intrinsic differences with the I Zw 1 template. Since we modelled the observed Fe II λ4570 blend (uncorrected for internal reddening), the actual R$_{\rm FeII}$ could be somewhat higher than reported (but not dramatically so).

PG 1351+640 ≡ J13532+6345 and PG 1411+441 ≡ J14138+4400. They are mini-BAL QSOs, with the absorption eating up the C IVλ1549 line core at $\Delta v_{\rm r} \approx -$ 5000 km s^{-1}(less than the emission blue wing zero intensity width). W(C IVλ1549) has been estimated mirroring the red side of the profile, agrees very well with the remaining emission blue wing at $\Delta v_{\rm r} \lesssim -5000$ km s^{-1} (§ 3.2).

Mrk 486 ≡ J15366+5433. Mrk 486 shows a similar absorption pattern as in PG 1351+640 and PG 1411+441 in a 1984 *IUE* spectrum which is apparently no longer present in more recent (1993) *HST*/FOS observations (see Fig. 3 where the profiles observed at different epochs are superimposed). However, the relatively poor S/N of the *HST* spectrum makes it difficult to ascertain whether the change in the mini-BAL absortion feature is real.

PG1552+085 ≡ J15547+0822. This source shows a BALnicity index ≈ 0 km s^{-1}. We include this source among the classical BAL QSOs because of its wide (albeit somewhat shallow) absorption trough. An *IUE* spectrum has been published by Turnshek et al. (1997), and retrieved by us. The new STIS spectrum confirms the BAL nature of the source, even if the feature, for CIVλ1549 is shallower and affected by noise since CIVλ1549 is close to the edge of the STIS covered spectral range.

PG 1700+518 ≡ J17014+5149. PG 1700+518 is the prototype low redshift BAL QSO. The UV spectral properties are remarkably similar to the ones of Mrk 231, PG 0043+054, and IRAS 0759+6459.

PG 2112+059 ≡ J21148+0607. This objects has a CIVλ1549 emission profile similar to the one of I Zw 1, and we observe a fully detached absorption trough. Optical lines are significantly broader than in NLSy1s, but the object still lies within the Pop. A area.

REFERENCES

Angonin, M.-C., Vanderriest, C., Remy, M., & Surdej, J. 1990, A&A, 233, L5

Arav, N., Li, Z., & Begelman, M. C. 1994, ApJ, 432, 62

Bachev, R., Marziani, P., Sulentic, J. W., Dultzin-Hacyan, D., & Calvani, M. 2004, ApJ, 617, 171

Barlow, T. A., Hamann, F., & Sargent, W. L. W. 1997, in ASP Conf. Ser. Vol. 128, Mass Ejection from Active Galactic Nuclei, eds. N. Arav, I. Shlosman, & R. J. Weymann (San Francisco: ASP), 13

Barvainis, R., Maloney, P., Antonucci, R., & Alloin, D. 1997, ApJ, 484, 695

Bechtold, J., Dobrzycki, A., Wilden, B., Morita, M., Scott, J., Dobrzycka, D., Tran, K., & Aldcroft, T. L. 2002, ApJS, 140, 143

Becker, R. H., Gregg, M. D., Hook, I. M., McMahon, R. G., White, R. L., & Helfand, D. J. 1997, ApJ, 479, L93

Becker, R. H., White, R. L., Gregg, M. D., Brotherton, M. S., Laurent-Muehleisen, S. A., & Arav, N. 2000, ApJ, 538, 72

Blandford, R. D., & Znajek, R. L. 1977, MNRAS, 179, 433

Boroson, T. A. 2002, ApJ, 565, 78

Boroson, T. A., & Green, R. F. 1992, ApJS, 80, 190

Boroson, T. A., & Meyers, K. A. 1992, ApJ, 397, 442

Brandt, W. N., Laor, A., & Wills, B. J. 2000, ApJ, 528, 637

Brotherton, M. S., van Breugel, W., Smith, R. J., Boyle, B. J., Shanks, T., Croom, S. M., Miller, L., & Becker, R. H. 1998, ApJ, 505, L7

Canalizo, G. & Stockton, A. 2002, in ASP Conf. Ser. Vol. 255, Mass Outflow in Active Galactic Nuclei: New Perspectives, eds. D. M. Crenshaw, S. B. Kraemer, & I. M. George (San Francisco: ASP), 195

Crenshaw, D. M., Kraemer, S. B., Turner, T. J., et al. 2002, ApJ, 566, 187

Crenshaw, D. M., Kraemer, S. B., & George, I. M. 2003, ARA&A, 41, 117

de Vaucouleurs, G., de Vaucouleurs, A., Corwin, H. G., Buta, R. J., Paturel, G., & Fouque, P. 1991, Volume 1-3, XII, 2069 pp. 7 Figs. (Berlin,Heidelberg,New York: Springer-Verlag)

Dultzin-Hacyan, D., Marziani, P., & Sulentic, J. W. 2000, RevMexAA Ser., Conf., 9, Astrophysical Plasmas: Codes, Models, and Observations, eds. S. J. Arthur, N. Brickhouse, & J. Franco (Mexico City: Inst. Astron., UNAM), 308

Elvis, M. 2000, ApJ, 545, 63

Espey, B. R., Carswell, R. F., Bailey, J. A., Smith, M. G., & Ward, M. J. 1989, ApJ, 342, 666

Falco, E. E., Kurtz, M. J., Geller, M. J., et al. 1999, PASP, 111, 438

Forster, K., & Halpern, J. P. 1996, ApJ, 468, 565

Gammie, C. F., Shapiro, S. L., & McKinney, J. C. 2004, ApJ, 602, 312

Ganguly, R., Bond, N. A., Charlton, J. C., Eracleous, M., Brandt, W. N., & Churchill, C. W. 2001, ApJ, 549, 133

Gaskell, C. M. 1982, ApJ, 263, 79

Green, P. J., Aldcroft, T. L., Mathur, S., & Schartel, N. 1997, ApJ, 484, 135

Hartig, G. F., & Baldwin, J. A. 1986, ApJ, 302, 64

Hewett, P. C., & Foltz, C. B. 2003, AJ, 125, 1784

Hill, G. J., Thompson, K. L., & Elston, R. 1993, ApJ, 414, L1

Hughes, S. A., & Blandford, R. D. 2003, ApJ, 585, L101

Jannuzi, B. T., Bahcall, J. N., Bergeron, J., et al. 1998, ApJS, 118, 1

Kerber, F., & Rosa, M. 2000, ST-ECF Newsletter, 27, 4

Korista, K. T., Voit, G. M., Morris, S. L., & Weymann, R. J. 1993, ApJS, 88, 357

Landolt, A. U. 1992, AJ, 104, 340

Lanzetta, K. M., Wolfe, A. M., & Turnshek, D. A. 1987, ApJ, 322, 739

Laor, A. & Brandt, N. 2002, in ASP Conf. Ser. Vol. 255, Mass Outflow in Active Galactic Nuclei: New Perspectives, eds. D. M. Crenshaw, S. B. Kraemer, & I. M. George (San Francisco: ASP), 99

Lípari, S., Colina, L., & Macchetto, F. 1994, ApJ, 427, 174

Lípari, S., Dottori, H., Mediavilla, E., et al. 2004, in IAU Symp. 217, Recycling Intergalactic and Interstellar Matter, eds. P. A. Duc, J. Braine, & E. Brinks (San Francisco: ASP), 302

Lobanov, A. P., & Roland, J. 2004, ArXiv Astrophysics e-prints, astro-ph/0411417

Marziani, P., Sulentic, J. W., Dultzin-Hacyan, D., Calvani, M., & Moles, M. 1996, ApJS, 104, 37 (M96)

Marziani, P., Sulentic, J. W., Zamanov, R., Calvani, M., Dultzin-Hacyan, D., Bachev, R.,& Zwitter, T. 2003a, ApJS, 145, 199 (M03)
Marziani, P., Sulentic, J. W., Zwitter, T., Dultzin-Hacyan, D., & Calvani, M. 2001, ApJ, 558, 553
Marziani, P., Zamanov, R., Sulentic, J. W., & Calvani, M. 2003c, MNRAS, 345, 1133
Marziani, P., Zamanov, R., Sulentic, J. W., Dultzin-Hacyan, D., Bongardo, C., & Calvani, M. 2003b, in ASP Conf. Ser. Vol. 290, Active Galactic Nuclei: From Central Engine to Host Galaxy, eds. S. Collin, F. Combes, & I. Shlosman (San Francisco: ASP), 229
Mathur, S. 2000, MNRAS, 314, L17
McIntosh, D. H., Rieke, M. J., Rix, H.-W., Foltz, C. B., & Weymann, R. J. 1999, ApJ, 514, 40
Najita, J., Dey, A., & Brotherton, M. 2000, AJ, 120, 2859
Narayanan, D., Hamann, F., Barlow, T., Burbidge, E. M., Cohen, R. D., Junkkarinen, V., & Lyons, R. 2004, ApJ, 601, 715
Pounds, K. A., Done, C., & Osborne, J. P. 1995, MNRAS, 277, L5
Reichard, T. A., Richards, G. T., Hall, P., et al. 2003, AJ, 126, 2594
Richards, G. T., Laurent-Muehleisen, S. A., Becker, R. H., & York, D. G. 2001, ApJ, 547, 635
Richards, G. T., York, D. G., Yanny, B., Kollgaard, R. I., Laurent-Muehleisen, S. A., & vanden Berk, D. E. 1999, ApJ, 513, 576
Sanders, D. B., Soifer, B. T., Elias, J. H., Madore, B. F., Matthews, K., Neugebauer, G., & Scoville, N. Z. 1988, ApJ, 325, 74
Schmidt, M., & Green, R. F. 1983, ApJ, 269, 352
Solomon, P. M., Downes, D., Radford, S. J. E., & Barret, J. W. 1997, ApJ, 478, 144
Sulentic, J. W., Marziani, P., & Calvani, M. 1998, ApJL, 497, L65
Sulentic, J. W., Marziani, P., & Dultzin-Hacyan, D. 2000a, ARA&A, 38, 521
Sulentic, J. W., Marziani, P., Zamanov, R., Bachev, R., Calvani, M., & Dultzin-Hacyan, D. 2002, ApJ, 566, L71
Sulentic, J. W., Marziani, P., Zwitter, T., Dultzin-Hacyan, D., & Calvani, M. 2000b, ApJ, 545, L15
Sulentic, J. W., Repetto, P., Marziani, P., Stirpe, G. M., Dultzin-Hacyan, D., & Calvani, M. 2005, A&A, submitted
Sulentic, J. W., Stirpe, G. M., Marziani, P., Zamanov, R., Calvani, M., & Braito, V. 2004, A&A, 423, 121
Sulentic, J. W., Zamfir, S., Marziani, P., Bachev, R., Calvani, M., & Dultzin-Hacyan, D. 2003, ApJ, 597, L17
Turnshek, D. A. 1986, in IAU Symp. 119, Quasars, eds. G. Swarup, & V. G. Kapahi (Dordrecht: Reidel), 119, 317
Turnshek, D. A., Grillmair, C. J., Foltz, C. B., & Weymann, R. J. 1988, ApJ, 325, 651
Turnshek, D. A., Monier, E. M., Sirola, C. J., & Espey, B. R. 1997, ApJ, 476, 40
Verner, E. M., Verner, D. A., Korista, K. T., Ferguson, J. W., & Ferland, G. J. 1999, ApJS, 120, 101
Vestergaard, M. 2003, ApJ, 599, 116
Vestergaard, M., & Wilkes, B. J. 2001, ApJS, 134, 1
Wise, J. H., Eracleous, M., Charlton, J. C., & Ganguly, R. 2004, ApJ, 613, 129
Weymann, R. J., Morris, S. L., Foltz, C. B., & Hewett, P. C. 1991, ApJ, 373, 23
Wills, B. J., Brandt, W. N., & Laor, A. 1999, ApJ, 520, L91
Yuan, M. J. & Wills, B. J. 2003, ApJ, 593, L11
Zamanov, R. & Marziani, P. 2002, ApJ, 571, L77
Zamanov, R., Marziani, P., Sulentic, J. W., Calvani, M., Dultzin-Hacyan, D., & Bachev, R. 2002, ApJ, 576, L9

Christian Bongardo, Valentina Braito, Massimo Calvani, and Paola Marziani: Istituto Nazionale di Astrofisica, Osservatorio Astronomico di Padova, Vicolo dell' Osservatorio 5, I-35122 Padova, Italy (bongardo@pd.astro.it; calvani@pd.astro.it; marziani@pd.astro.it; zamanov@pd.astro.it).
Deborah Dultzin-Hacyan: Instituto de Astronomía, UNAM, Apdo. Postal 70−264, 04510 México, D. F., México (deborah@astroscu.unam.mx).
Jack W. Sulentic: Department of Physics and Astronomy, University of Alabama, Tuscaloosa, AL 35487, USA (giacomo@merlot.astr.ua.edu).
Radoslav K. Zamanov: National Astronomical Observatory Rozhen, POB 136, Smoljan, BG-4700, Bulgaria.